Materials Science & Engineering A 819 (2021) 141527

Contents lists available at ScienceDirect

Materials Science & Engineering A

journal homepage: www.elsevier.com/locate/msea

Experimental investigation into microstructure, mechanical properties, and cracking mechanism of IN713LC processed by laser powder bed fusion

M. Mohsin Raza, Yu-Lung Lo *

National Cheng Kung University, Department of Mechanical Engineering, Tainan, Taiwan

ARTICLE INFO

Keywords:
Laser powder bed fusion
IN713LC
Solidification cracking
Ductility dip cracking

ABSTRACT

IN713LC is a Ni-based superalloy with extensive uses in the aerospace industry. However, fabricating IN713LC components using additive manufacturing technologies such as laser powder bed fusion (LPBF) is extremely challenging due to its high composition of alloying elements (e.g., Al and Ti), which increase its susceptibility to cracking. Accordingly, the present study conducts an experimental investigation into the LPBF processing parameters (i.e., laser power and scanning speed) which enable the fabrication of LPBF IN713LC parts with a high relative density and minimal cracking. The effects of heat treatment on the microstructure and mechanical properties of the as-built parts are then examined. The results show that IN713LC is prone to the two microcracking mechanisms, namely solidification cracking due to the formation of low-melting-point elements at the grain boundaries and ductility dip cracking (DDC) as a result of grain boundary sliding. However, given an appropriate selection of the LPBF processing conditions, as-built IN713LC components with an average yield strength of 800 MPa, an ultimate tensile strength of 998 MPa, and ultimate elongation of 12.5% at room temperature are better than those of as-cast IN713LC specimens. Notably, the solid solution heat treatment process yields a significant improvement in the yield strength compared to that of the as-built sample. Moreover, all the mechanical properties of the sample processed by solid solution heat treatment are comparable to those of the as-cast IN713LC sample.

1. Introduction

Laser powder bed fusion (LPBF) has many advantages over traditional machining methods including a faster manufacturing time, a lower production cost, and the ability to produce near-net-shaped parts without the need for additional machining. As a result, it is widely used throughout the aerospace, medical and automotive industries for the production of turbines, surgical instruments, structural components, and so on. However, there are still several major challenges to be overcome in using LPBF including improved dimensional accuracy, surface roughness, and mechanical properties (e.g., lower porosity, higher yield strength, and better crack resistance). Within the aerospace industry, many components such as the turbines and rotors have to be operated at extremely high temperature over 650 °C. Therefore, the choice of appropriate materials with good creep resistance, high tensile strength, and good oxidation resistance is essential in ensuring the mechanical integrity and reliability of the engine under typical working conditions. Among various alloys suitable for these applications including IN718, IN738, and Hastelloy, IN713LC alloy is one of the most commonly used due to its favorable properties at the extreme working conditions and also offers better resistance against creep and oxidation.

Although numerous mechanisms help strengthen IN713LC at high temperature, the main strengthening phase is γ' coherent precipitates (an inter-metallic Ni3 (Al, Ti) compound) within the γ matrix [1]. The development of $M_{23}C_6$ carbides at the grain boundaries also imbues the alloy with high strength and ductility by impeding grain boundary sliding [2]. Henderson et al. [3] examined the weldability of a wide range of Ni-based superalloys and found that alloys with an Al + Ti composition of less than 2.5 wt% are more amenable to welding than those which do not. IN713LC has an Al + Ti composition of more than 6 wt% and is thus classified as non-weldable compared to IN718, which has an Al + Ti composition of just 1.5 wt%. LPBF has a similar forming mechanism to that of welding. Consequently, many materials that are considered as non-weldable are also regarded as non-printable in the LPBF process. Harrison [4] investigated the LPBF process of Ni-based superalloys and found that the crack susceptibility of the alloy could be quantified by the ratio of the apparent thermal stress to the solid solution strength (SSS). In particular, the susceptibility of the alloy

* Corresponding author.
E-mail address: loyl@mail.ncku.edu.tw (Y.-L. Lo).

https://doi.org/10.1016/j.msea.2021.141527
Received 8 February 2021; Received in revised form 7 May 2021; Accepted 25 May 2021
Available online 29 May 2021

Table 1
IN713LC chemical composition (wt.%).

Ni	Al	Co	Cr	Fe	Mn	Mo	Nb + Ta	Si	Ti	C
Bal.	6.15	0.35	11.65	0.07	0.001	4.06	2.04	0.152	0.774	0.0453

toward cracking increased as the ratio approached zero. For IN713LC alloy, the ratio has a value of approximately 0.2. Thus, it is regarded as a high crack-susceptibility material.

The LPBF process is associated with many micro-cracking mechanisms including solidification cracking and liquation cracking [5], which are the result of a locally reduced solidus temperature due to segregation in the liquid during solidification or the presence of low-melting-point phases in the solid heat-affected zone (HAZ), respectively. Ductility dip cracking (DDC) [6] may also occur due to accumulated strain (dislocation pile-up) at the grain boundaries as a result of transient thermal stresses. Furthermore, for Ni-based superalloys, strain age cracking (SAC) [7] readily takes place during solid solution heat treatment due to a precipitation of strengthening phase, especially γ'-Ni_3M, during the ramp stage. It leads to a significant loss of ductility and inhibits the ability of the material to release the residual stress generated during processing or in the precipitation process itself (lattice mismatch). With its high susceptibility toward cracking, IN713LC is conventionally regarded as unsuitable for welding or LPBF processing. Thus, IN713LC components are generally formed by investment casting.

Accordingly, the present study conducts an experimental investigation into the LPBF processing of IN713LC components with a high relative density and minimal cracking. LPBF trials are first performed to fabricate simple IN713LC cubic structures at scanning speeds ranging from 400 to 850 mm/s and laser powers of 110–300 W. Based on an inspection of the relative density and cracking density of the as-built components, two specific combinations of the scanning speed and laser power are chosen to fabricate further cubic structures and tensile test specimens for microstructural analysis and mechanical evaluation, respectively. The microstructure, grain size, chemical composition, and mechanical properties are systematically explored for both the as-built parts and as-built parts processed by solid solution heat treatment or stabilization heat treatment, respectively. The mechanical properties of the tensile test specimens are compared with those of as-cast IN713LC specimens with the same geometry and dimensions. In addition, an investigation is performed into the correlation between the grain size and the mechanical properties of the as-built and heat-treated specimens. Finally, a detailed inspection of the cracking characteristics of the as-built parts is conducted to identify the main cracking mechanisms involved in the LPBF processing of IN713LC.

2. Material and methods

2.1. IN713LC powder

IN713LC powder with a particle size distribution of $D_{10} = 16.25$ μm, $D_{50} = 30.49$ μm, and $D_{90} = 51.31$ μm was used to conduct the experiments. According to the supplier's specification (Tong Tai Company, Taiwan), the powder had the chemical composition as shown in Table 1.

2.2. LPBF processing of IN713LC

In the LPBF processing, the ability of the powder to form a uniformly distributed layer over the powder bed has a great effect on the porosity, cracking, and mechanical properties of the built part. Accordingly, the flowability of the powder particles should be enhanced prior to the deposition process. In the present study, this was achieved by first sieving the as-supplied powder using a 200 mesh in order to remove any large element and then drying the remaining powder in a vacuum oven at 100 °C for 12 h in order to remove any surface contamination such as moisture.

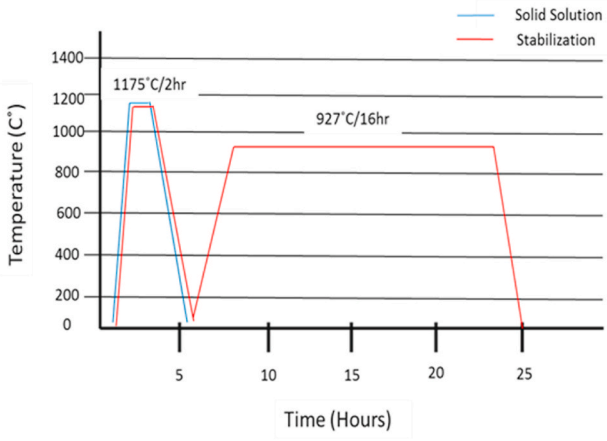

Fig. 1. Schematic diagram of the heat-treatment profiles for IN713LC specimens.

The LPBF trials were conducted using a Tongtai AM-250 selective laser melting (SLM) machine equipped with a CW Nd: YAG laser with a wavelength of 1064 nm, the maximum power of 500 W, and the maximum scanning speed of 2000 mm/s. To prevent oxidation, all of the experiments were performed in a nitrogen environment with an oxygen concentration of less than 1000 ppm. The layer thickness was set as 40 μm while the hatch spacing was set as 100 μm. In addition, the laser scanning process was performed using a zig-zag strategy with a rotation angle of 67° between layers. The mechanical properties of LPBF-processed parts are dependent on many factors including the laser power, the scanning speed, the hatch spacing, and the scanning strategy [8]. However, as in previous studies, the present experiments are focused only on the effects of the laser power and scanning speed, respectively. In performing the LPBF trials, two different components were fabricated, namely cubic structures with the dimensions of 10 × 10 × 10 mm^3 and tensile test specimens with the dimensions shown in Section 3.2.

2.3. Heat treatment of IN713LC parts

Following the LPBF printing trials, some of the parts were left in an as-built condition while others were heat-treated in a muffle oven at a temperature of 1175 °C for 2 h (solid solution heat treatment) or solution heat-treated at 1175 °C for 2 h, and then reheated to 927 °C at a rate of 10 °C per minute and aged for a further 16 h (stabilization heat treatment (see Fig. 1). Note that air cooling was performed after each heat-treatment process. In other words, three different LPBF samples were obtained for investigation purposes, namely, as-built, solid solution heat-treated, and stabilization heat treated samples. It is noted that the heat-treatment conditions used in this study are identical to those considered in Refs. [9,10] for the casting IN713LC components to observe the effect of heat treatment.

2.4. Microstructural analysis and mechanical testing of IN713LC samples

Samples for microstructural analysis were sectioned perpendicularly (XY-plane) to the build direction with a water-cooled cut-off machine and then mounted in epoxy resin. The mounted samples were grinded

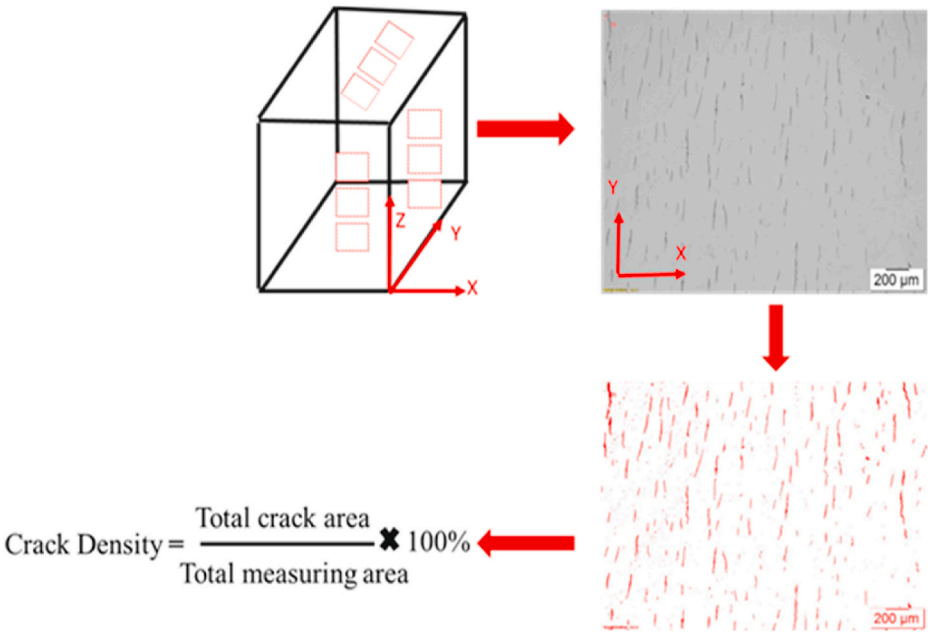

Fig. 2. Schematic representation of crack density evaluation process.

with SiC sandpaper down to a grit size of P200–P3000 and were then polished further with diamond suspension down to 0.3 μm sizing. Following the grinding and polishing processes, the samples were cleaned in ethanol to remove surface debris and contaminants. The features of microstructure such as grain size, grain shape, grain orientation, texture, and composition were examined by the scanning electron microscopy (SEM), optical microscopy (OM), and energy-dispersive X-ray spectrometry (EDS) equipped with electron backscattered diffraction (EBSD) (ZEISS Supra 55). Prior to the observation process, the samples were polished by ion bombardment in order to remove the stress generated during the mechanical polishing operation and to generate higher Kikuchi patterns. The working distance of 12 mm between the sample and EBSD detector, the step size of 0.7 μm, and the accelerating voltage of 20 kV were used. The mechanical properties of the various as-built, solid solution heat-treated, and stabilization heat-treated test samples were evaluated using a universal tensile test machine (HT-8336, Hung Ta, Taiwan) at room temperature. The tensile test rate of 1 mm min^{-1} and the initial strain rate of 8.33×10^{-4} S^{-1} are used for tensile tests [11]. The dimension of the tensile test specimen was designed according to the ASTM standard E8/E8M [12] and was slightly modified to fit with the configuration of the universal test machine. The mechanical properties of the samples were then compared with those of as-cast IN713LC samples [13].

2.5. Crack density evaluation of as-built IN713LC samples

The crack density of the as-built LPBF cubic structures was evaluated using an optical microscope (Olympus BX51 M) and image-processing software. Briefly, OM images were acquired of the top surface, side surface, and cross-sectional plane of each sample. As shown in Fig. 2, OM images were obtained from three different regions of each plane (indicated by the red rectangles). Furthermore, within each region, two images were acquired at randomly selected locations. For each image, the total crack area was measured using Image J software and the crack density was then computed as the total crack area divided by the total measuring area. The crack density measurements obtained for the 18 images were then averaged to obtain a representative value for the sample and a similar method is used to calculate the relative density of the samples. Note that as-built samples containing an excessive number of pores were excluded from the measurement process since Image J cannot perfectly differentiate between pores and cracks.

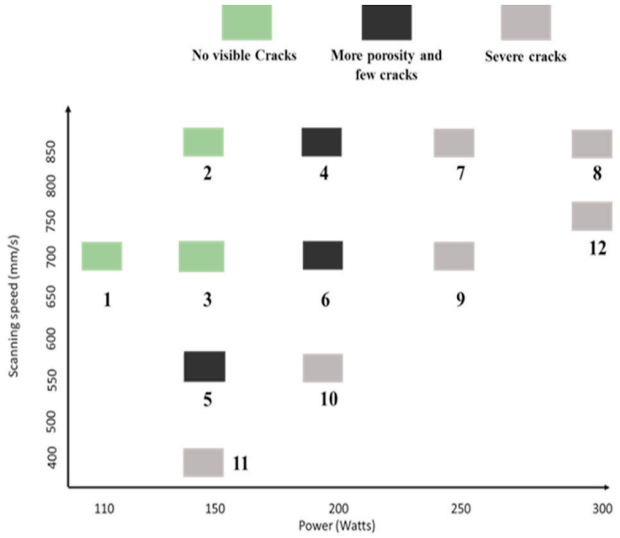

Fig. 3. Schematic representation of processing map used in this study for IN713LC samples.

3. Experiment and methods

3.1. Construction of processing map for IN713LC

Although there are various methods, i.e., design of experiment (DOE) and linear energy distribution (LED) [14,15], for choosing the process parameters with experiments, however, an experimental investigation into the LPBF processing of IN713LC components with high relative density and low crack density is conducted using 1D energy density approach in this study. Similar approaches [16,17] are also used to conduct the experiments for Ni-based superalloys in order to find the optimal processing parameters.

Three-dimensional IN713LC cubes were printed using the laser power in the range from 110 to 300 W and the scanning speed in the

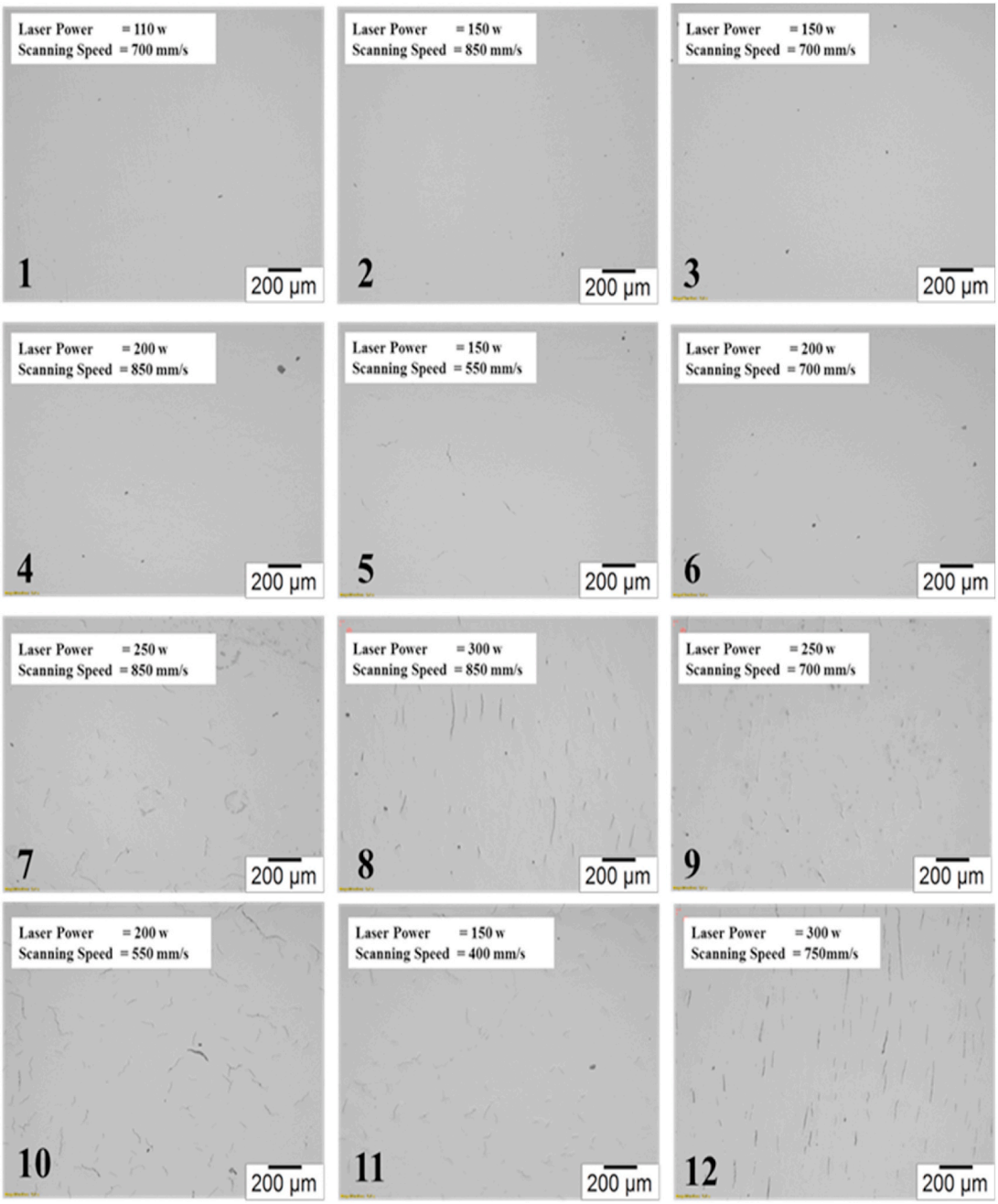

Fig. 4. OM micrographs showing the effect of laser parameters on IN713LC from Samples #1 to #12.

range from 400 to 850 mm/s. After excluding the samples with excessive cracking, a total of just 12 samples, as shown in Fig. 3, were remained. As a result, the cracks observed by the OM images were presented in Fig. 4. In general, the experimental results confirm that it is difficult to fabricate IN713LC parts with no cracks, low porosity, and minimal warpage using the LPBF process. However, out of the 12 samples shown in Fig. 3, Samples #1 to #3 (shown as green boxes) were found to exhibit a smooth and crack-free surface with good bonding to the substrate while Samples #4 to #6 were found to have relatively high porosity but few cracks (shown as black boxes). Also, it is found that Samples #7 to #12 (shown as grey boxes) have the severe cracks. From all samples, the cracks inside Samples #7 to #12 as shown in Fig. 4 are so severe, and their cubes cannot be built successfully because of the extra melting and wrapping in processing. As a result, the LPBF processing parameters for only Samples #1 to #6 with calculated crack density and relative

Table 2
Effects of LPBF processing conditions on relative density and crack density of as-built IN713LC parts.

Number	Power (W)	Scanning Speed (mm/s)	1D Energy Density (J/mm)	Relative Density	Crack Density ($(mm^2/mm^2) \times 100\%$)
#1	110	700	0.157	99.95%	0.011%
#2	150	850	0.176	99.92%	0.015%
#3	150	700	0.214	98.57%	0.028%
#4	200	850	0.235	97.56%	0.077%
#5	150	550	0.273	97.23%	0.088%
#6	200	700	0.286	96.53%	0.103%

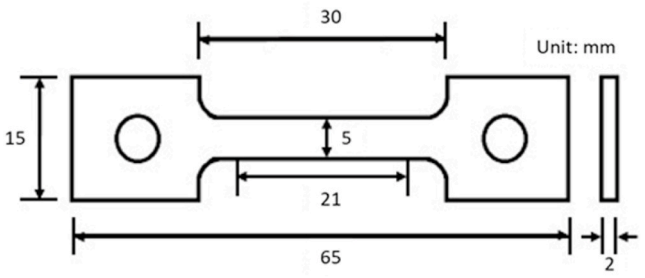

Fig. 5. Configuration of tensile test specimen used in this study.

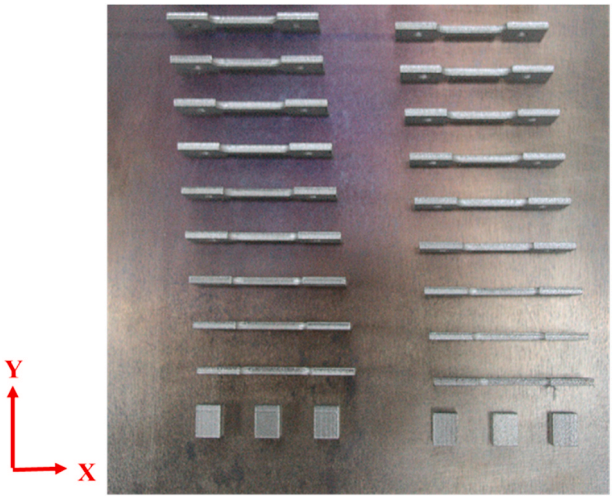

Fig. 6. Photograph of LPBF specimens after the built for tensile test and cubic specimens.

density are studied and presented in Table 2.

An inspection of Table 2 reveals that as the laser energy density in the LPBF process increases, the crack density increases while the relative density decreases. Thus, the optimal part quality, i.e., the highest relative density (99.95%) and lowest crack density (0.011%), is obtained using a laser power of 110 W and scanning speed of 700 mm/s corresponding to an energy density of 0.157 J/mm (see Sample #1 in Table 2). It is noted that the present findings are consistent with those of Perevoshchikova et al. [8] reported that non-printable Ni-based superalloys can be processed by LPBF provided that the energy density is suitably controlled.

3.2. Microstructure and mechanical properties of LPBF-printed IN713LC components

Based on the results presented in Table 2, just two LPBF processing conditions (referred to hereafter as Sample #1 and Sample #2, respectively) were selected for further analysis purposes. For each set of processing conditions, two different types of components were fabricated, namely cubic structures with the dimensions of $10 \times 10 \times 10$ mm^3 and tensile test specimens with the geometry and dimensions shown in Fig. 5. For the cubic structures, three samples, namely as-built, solid solution heat-treated, and stabilization heat-treated samples, were prepared for each set of LPBF processing conditions. The samples were then characterized by SEM, EDS, and EBSD, as described previously in Subsection 2.4. For the tensile test specimens, a total of nine samples were prepared for each set of LPBF processing parameters in order to evaluate the average and standard deviation properties of the samples, i.e., three specimens for each condition (i.e., as-built, solid solution heat-treated, and stabilization heat-treated specimens). Fig. 6 shows two sets of LPBF parts produced under the Sample #1 condition (left) and Sample #2 condition (right).

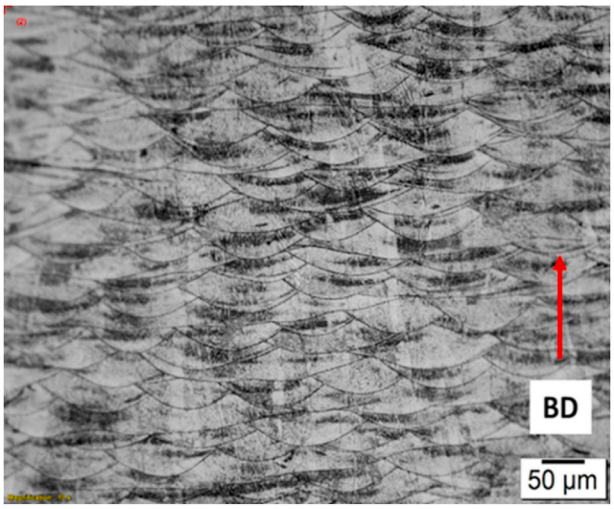

Fig. 7. OM image showing the microstructure of as-built IN713LC cubic specimen.

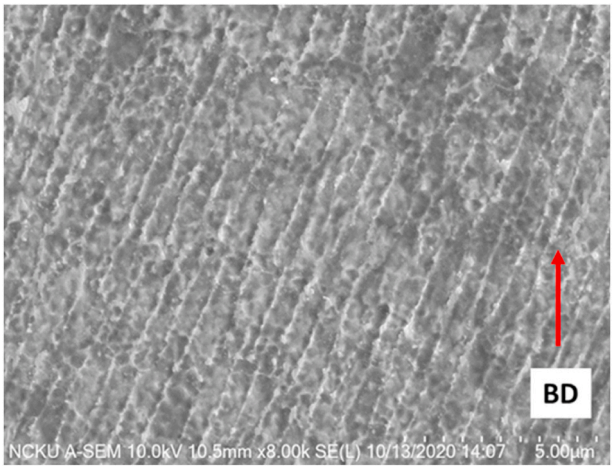

Fig. 8. SEM image showing the microstructure of as-built IN713LC cubic specimen.

4. Results and discussions

4.1. Microstructure of as-built IN713LC cubes

Fig. 7 presents an OM image of the vertical cross-section of the as-built cubic structure. (Note that Samples #1 and #2 were found to have very similar microstructures, and hence Sample #1 is chosen arbitrarily for an illustration purpose here.) It can be seen that the cut ends of the melted tracks have the form of arcs due to the Gaussian energy distribution of the laser. Furthermore, the cut ends of the melted tracks are packed closely together, which indicates a good metallurgical bonding between the layers. It is noted that these findings are consistent with those presented in a previous study for LPBF-processed IN718 [18].

Fig. 8 presents a high-magnification SEM image of the same cross-section. The image shows that the low laser energy density (i.e., 0.157 J/mm) in the LPBF process results in a high cooling rate. In particular, during the cooling stage of the melting and solidification process, heat transfer occurs predominantly in the negative build direction due to the cooling effect of the substrate. In Fig. 8, due to the

Fig. 9. EBSD image showing grain orientation in three planes for the as-built IN713LC cubic specimen.

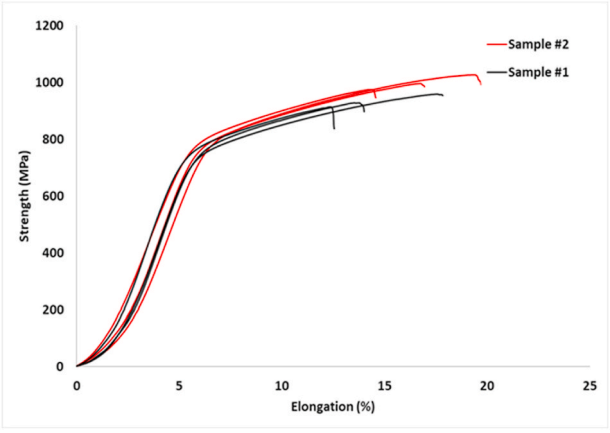

Fig. 10. Tensile test results for as-built Samples #1 and #2 conducted at room temperature.

high temperature gradient and solidification rate in the Z-direction, the dendrite growth and grain formation also show a strong orientation toward the Z-direction.

In addition, Fig. 9 shows a three-dimensional EBSD image of the as-built IN713LC cubic specimen. The image confirms that the grains on the side of the cube have a columnar structure with a strong Z-axis growth orientation. Moreover, the top surface consists of equiaxed grains. During LPBF processing, the heat flow direction and thermal gradient in the laser melted tracks are complicated, and hence the microstructure growth is also complex [19]. This tendency is clearly visible in the results presented in Fig. 9, in which the columnar and equiaxed grains have different crystallographic orientations (as indicated by the different colors).

A close inspection of Fig. 9 shows that most of the grains on the XY plane are oriented in the (001) and (101) directions. Moreover, the average grain size on the top surface is around 25–35 μm. Meanwhile, the majority of the grains on the YZ and XZ planes are columnar grains with a size ranging from 45 to 125 μm. Most of the grains on the YZ plane are oriented in the (001) and (111) directions while most of those on the XZ plane are oriented in the (001) and (101) directions. As it can be seen that these grains are oriented in various crystallographic orientations, so it helps to impede the cracks to propagate, which resulted in the enhancement of mechanical properties. However, the YZ and XZ planes

Table 3
Mechanical properties of as-built IN713LC test pieces for (a) Sample #1 and (b) Sample #2.

Sample #1	YS (MPa)	UTS (MPa)	UE %	TE %
	757	958	13	13.3
	773	928	9	9.4
	758	913	7.8	8.1
Average	762	933	9.9	10.2
Standard Deviation	7	18	2.2	2.2
Sample #2	YS (MPa)	UTS (MPa)	UE %	TE %
	791	995	11.8	12.3
	796	973	9.8	10.2
	813	1026	16	16.3
Average	800	998	12.5	12.9
Standard Deviation	9	21	2.5	2.5

Table 4
Tensile properties of as-cast IN713LC [13].

	T (C°)	YS (MPa)	UTS (MPa)	Elongation %
As Cast	20	750	850	8.5

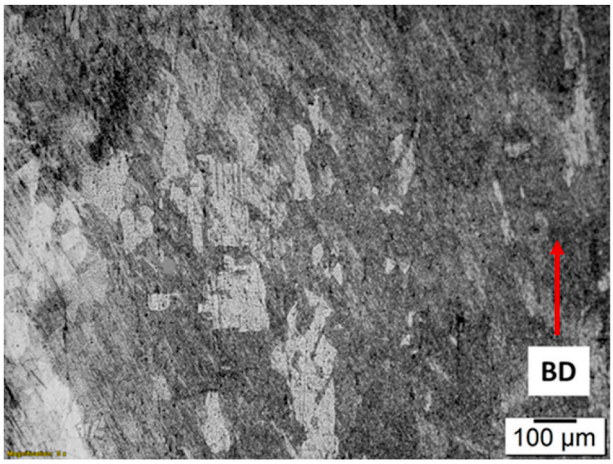

Fig. 11. OM image of the characteristic microstructure after heat treatment showing an increase in grain size.

also contain a small number of equiaxed grains with an average size of 10–25 μm and various crystal orientations. It is speculated that these small grains are the result of partial re-melting, epitaxy growth, and melt pool solidification kinetics [20]. In other words, during the LPBF process, a re-melting of the earlier layers occurs, which results in the strong epitaxial grain growth from one layer to the next and heat flow via conduction through the earlier layers and substrate in the Z-direction.

4.2. Mechanical properties of as-built IN713LC samples

One of the main objectives of the present study is to produce LPBF-printed IN713LC components with comparable mechanical properties to those of as-cast IN713LC parts. Fig. 10 shows the tensile test results obtained for the as-built IN713LC test pieces. Table 3 shows the measurement results obtained for the yield strength (YS), ultimate tensile strength (UTS), ultimate elongation (UE), and total elongation (TE) of Samples #1 and #2 (three specimens per sample). Table 4 shows the corresponding results for an as-cast IN713LC test piece [13]. Note that the test results relate to room temperature conditions in both cases. Comparing the results presented in Tables 3 and 4, it is seen that the mechanical properties of the as-built LPBF samples for both Sample #1 and Sample #2 are better than those of the as-cast sample. In particular,

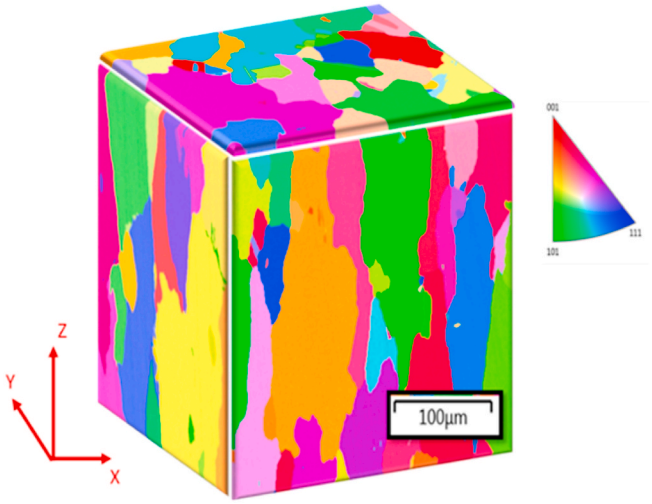

Fig. 12. EBSD image showing grain orientation in three planes after solid solution heat treatment.

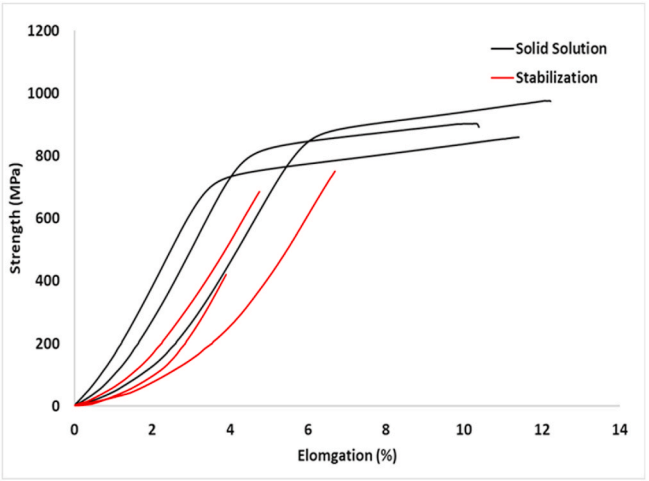

Fig. 13. Tensile test results for LPBF test specimens after two different heat treatments (solid solution and stabilization) conducted at room temperature.

the LPBF sample in Table 3(b) has an average yield strength of 800 MPa, an ultimate tensile strength of 998 MPa, and an ultimate elongation of 12.5%.

4.3. Microstructure of heat-treated IN713LC cubes

Fig. 11 presents an OM cross-sectional image of the IN713LC cube (Sample #1) following solid solution heat treatment. Comparing the image in Fig. 11 with that in Fig. 7 for the as-built cube, it is seen that the melt pool and cut ends of the melted tracks are no longer evident after the heat treatment process. Moreover, the grains become larger and coarser and only a few small grains remain.

Fig. 12 presents a three-dimensional EBSD image of the heat-treated cube. The results confirm that the grain size of the heat-treated cube is around 3–4 times larger than that of the as-built cube (see Fig. 9) due to the elevated temperature (1175 °C) used in the heat treatment process. For example, the grains on the top surface of the sample have a size of around 50–120 μm while those on the side surfaces have a size of around 140–230 μm. Most of the grains on the top surface change from equiaxed grains to large coarse grains. However, the grains on the side surfaces maintain a strong growth orientation in the build direction with predominantly (101) and (111) crystallographic orientations.

Table 5
Mechanical properties of LPBF test pieces after (a) solid solution heat treatment and (b) stabilization heat treatment.

(a) solid solution heat treatment				
Solid Solution	YS (MPa)	UTSm (MPa)	UE %	TE %
	892	973	7.2	7.6
	828	902	6.8	7.2
	734	858	8.7	9
Average	818	911	7.5	7.9
Standard Deviation	64	47	0.8	0.7
(b) stabilization heat treatment.				
Stabilization	YS (MPa)	UTS (MPa)	UE %	TE %
	685	**658**	**0**	**0**
	750	**750**	**0**	**0**
	421	**421**	**0**	**0**
Average	**618**	**609**	**0**	**0**
Standard Deviation	**142**	**138**	**0**	**0**

4.4. Mechanical properties of IN713LC samples after solid solution heat treatment and stabilization heat treatment

Fig. 13 shows the mechanical properties of the IN713LC tensile test specimens following solid solution heat treatment (1175 °C for 2 h) and stabilization heat treatment (927 °C for 16 h), respectively. Note that Fig. 13 shows the results obtained for three test specimens from Sample #1. (The results obtained from Sample #2 are very similar, and are omitted from the figure accordingly.) As a result, Table 5 shows the mechanical properties of three specimens following two heat treatment processes. It is seen that both heat treatment processes result in a significant reduction in the ultimate tensile strength (UTS), ultimate elongation (UE), and total elongation (TE) of the specimens compared to those of the as-built specimens (Table 4). The degradation in the mechanical properties is particularly apparent following the stabilization heat treatment. The yield strength (YS) also reduces following the prolonged aging at 927 °C. However, the solid solution heat treatment process yields a significant improvement in the yield strength compared to that of the as-built sample. Moreover, all of the mechanical properties of the sample processed by solid solution heat treatment are comparable to those of the as-cast IN713LC sample shown in Table 4.

Overall, the results presented in Table 5 indicate that the stabilization heat treatment process has a detrimental effect on the mechanical properties of the LPBF-printed IN713LC specimens. This finding is reasonable since the prolonged heating is at a temperature in the range of 900–1000 °C, it prompts the precipitation of γ′ phase, which impedes the release of the residual stress induced in the specimen during the heating and cooling process [6]. Also, the volume reduction effect associated with the precipitation of γ’ phase introduces further stress within the solidified component [21]. Collectively, the two stresses cause a significant loss in the ductility of the specimen. As a result, cracks readily form under tensile loading, and hence the mechanical properties are heavily degraded [6,17].

4.5. Effects of grain size on mechanical properties

Fig. 14(a) and (b) show the EBSD results for the top surfaces of the as-built and solid-solution heat-treated IN713LC cubes, respectively. The results confirm that the solid solution heat treatment process prompts a change in the grain structure from equiaxed grains with a size of around 25–35 μm to coarse grains with a size of around 50–120 μm. According to Wang et al. [17], the poor mechanical properties of non-weldable alloys processed by LPBF after the heat-treatment are the result mainly of a large grain size. Thus, the EBSD results presented in Fig. 14 suggest that the loss in mechanical properties of the present heat-treated IN713LC samples can also be attributed to a larger and coarser grain structure.

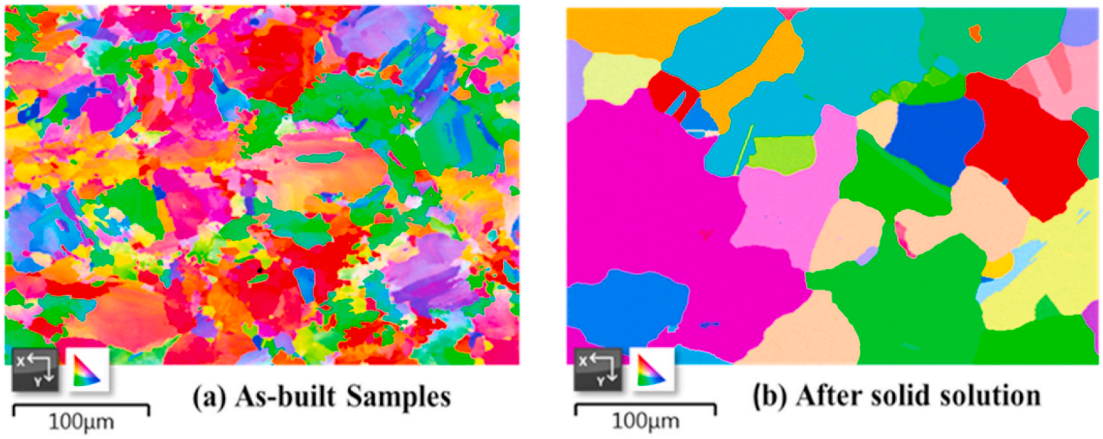

Fig. 14. EBSD showing grain size for (a) as-built IN713LC sample and (b) solid-solution heat-treated IN713LC sample.

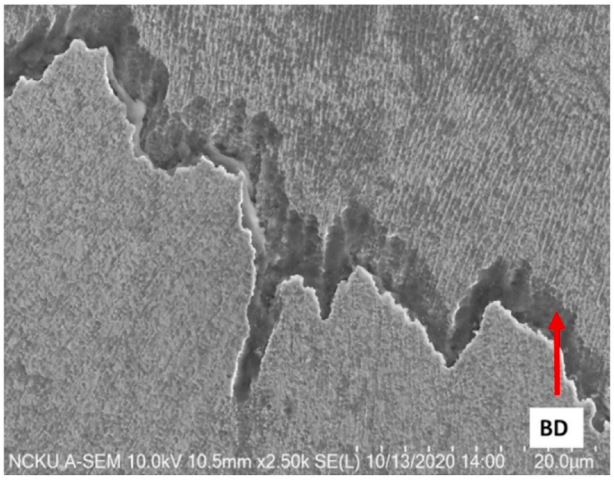

Fig. 15. Backscattered SEM image of a typical "jagged" crack in the build direction.

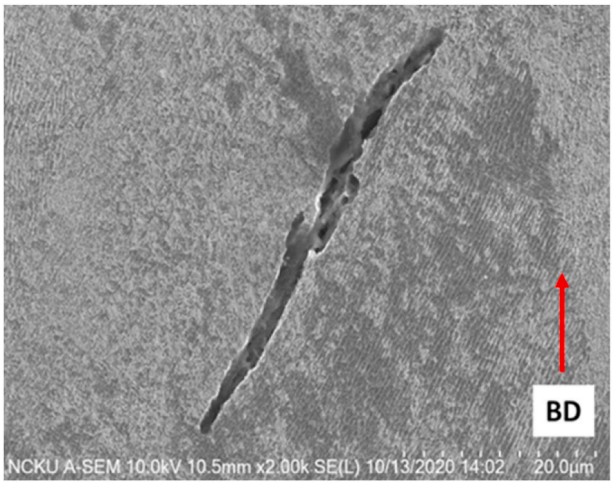

Fig. 16. Backscattered SEM image of a typical "straight" crack in the build direction.

4.6. Crack characterization of as-built IN713LC samples

To further explore the micro-cracking mechanism of the as-built IN713LC components, a detailed SEM and EDS analysis was performed

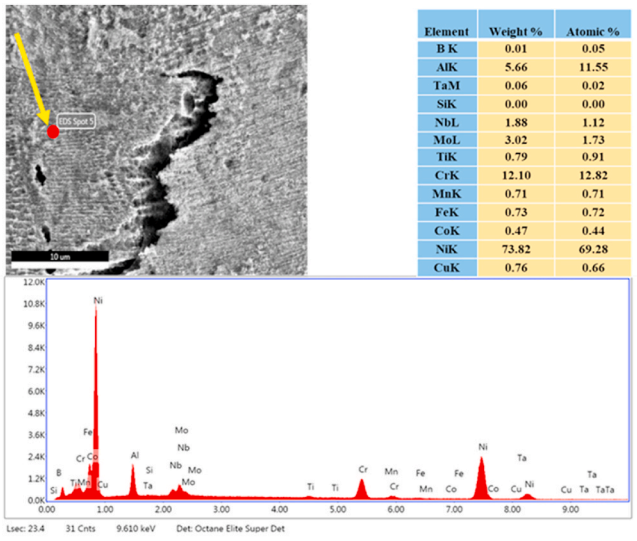

Element	Weight %	Atomic %
B K	0.01	0.05
AlK	5.66	11.55
TaM	0.06	0.02
SiK	0.00	0.00
NbL	1.88	1.12
MoL	3.02	1.73
TiK	0.79	0.91
CrK	12.10	12.82
MnK	0.71	0.71
FeK	0.73	0.72
CoK	0.47	0.44
NiK	73.82	69.28
CuK	0.76	0.66

(a)

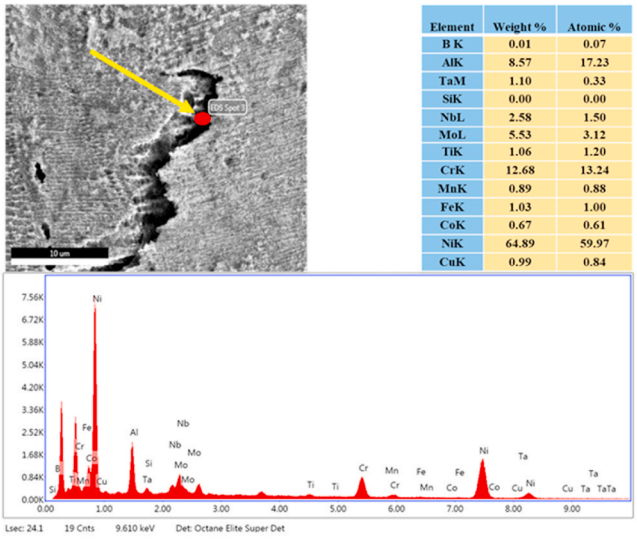

Element	Weight %	Atomic %
B K	0.01	0.07
AlK	8.57	17.23
TaM	1.10	0.33
SiK	0.00	0.00
NbL	2.58	1.50
MoL	5.53	3.12
TiK	1.06	1.20
CrK	12.68	13.24
MnK	0.89	0.88
FeK	1.03	1.00
CoK	0.67	0.61
NiK	64.89	59.97
CuK	0.99	0.84

(b)

Fig. 17. EDS analysis results for as-built IN713LC microstructure (a) outside the jagged crack (Spot 5) and (b) inside the jagged crack (Spot 3).

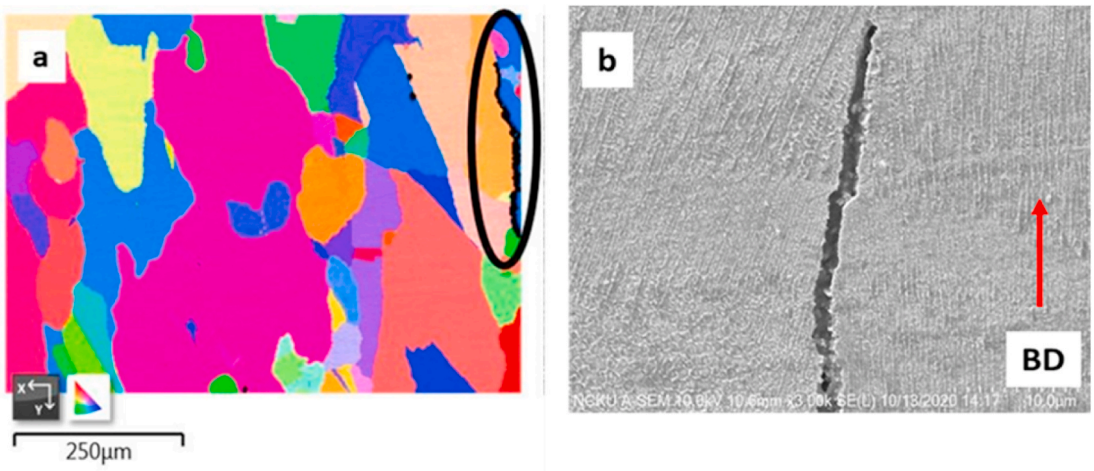

Fig. 18. (a) EBSD image and (b) magnified SEM image showing crack propagating near-parallel to the build direction and also close to grain boundary in as-built LPBF sample.

to study the micro-cracks formed in the vertical cross-section of the cube fabricated using Sample #1 LPBF processing conditions. As shown in Fig. 15, a jagged crack morphology was observed running across the cross-section with the crack features propagating in the build (i.e., grain elongation) direction. A straight crack morphology was also observed in Fig. 16. The straight crack also propagated in the build direction. However, in contrast to the jagged crack morphology, the crack passed only through the columnar dendrites at the grain boundaries.

The cracks shown in Figs. 15 and 16 resemble the solidification cracks reported by Carter et al. [21] in LPBF-processed Ni-based superalloy. The straight crack morphology is also consistent with that observed by Gao et al. [22] for TiAl9V0·5Y alloy processed by LPBF. It was suggested in Ref. [23] that the cracking effect in Ni-based superalloys can be inhibited by controlling the cooling rate in such a way as to promote the formation of equiaxed grains.

To confirm the nature of the cracks shown in Figs. 15 and 16, the chemical compositions of the cracks were examined by EDS. Fig. 17 shows the EDS results for the jagged crack morphology. As shown in Fig. 17(a), the region of the microstructure adjacent to the crack (i.e., Spot 5) has a chemical composition similar to that of original powder (see Table 1). However, crack itself (i.e., Spot 3) has higher concentration of Al, Cr, Nb, and Ti, as shown in Fig. 17(b). The present results are thus consistent with the findings of Rosenthal and West [24] that Al + Ti-rich areas prompt the formation of low-melting-point constituents such as $\gamma + \gamma'$ eutectic phases, which accelerate cracking. The EDS results obtained for the straight crack morphology similarly showed the existence of multiple chemical elements within the crack region of the sample. Note that the results are deliberately omitted here for the sake of conciseness. In other words, it is reasonable to assume that the straight cracks are also formed as the result of the precipitation of low-melting-point elements at the grain boundaries. The present observations are consistent with those of Chamanfar et al. [25], who reported that alloying elements readily form low-melting-point liquid films along the solidified grain boundaries during the electron beam welding of IN713LC and lead to solidification cracking when the accumulated tensile stress exceeds the local strength. Thus, overall, the present EDS analysis results confirm that the jagged cracks (Fig. 15) and straight cracks (Fig. 16) in the present LPBF-printed IN713LC parts are solidification cracks rather than cold cracks.

In addition to the solidification cracks described above, the EBSD and SEM analysis also revealed the presence of vertical cracks running near-parallel to the build direction, as illustrated in Fig. 18. The cracks are consistent with those reported by Ref. [21] and are thought to be the result of ductility dip cracking (DDC), in which the heat provided to the underlying layers of the built component in the LPBF process is insufficient to produce fully dynamic recrystallization, but leads instead to grain boundary sliding.

5. Conclusions and suggestions

This study has conducted an experimental investigation into the optimal LPBF processing conditions for the fabrication of as-built IN713LC parts with a high relative density and low cracking density. Having established the optimal LPBF processing conditions, a further investigation has been performed to examine the effects of heat treatment on the microstructure and mechanical properties of the as-built parts. Finally, SEM, OM, EBSD, and EDS techniques have been used to examine the correlation between the grain size and mechanical properties of the various samples and the cracking mechanisms in the as-built specimens. The main findings of this study can be summarized as follows.

- A lower laser energy density is beneficial in increasing the relative density of the as-built IN713LC components and reducing the crack density. Given the optimal processing conditions (a laser power of 110 W and a scanning speed of 700 mm/s), the relative density reaches as much as 99.95% while the crack density is just 0.011%. Moreover, the mechanical properties (e.g., the yield strength, ultimate tensile strength, and ultimate elongation) of the as-built sample are better than those of an as-cast sample of an equivalent geometry and size.
- The grains on the upper surface of the as-built IN713LC samples have an equiaxed structure while those on the side surfaces have a columnar structure oriented in the build direction. The equiaxed grains have an average size of 25–35 μm while the columnar grains have a size of 45–125 μm. However, following heat treatment, the average grain size on the top surface increases to 50–120 μm while that on the side surfaces increases to 140–230 μm.
- The larger grain size leads to a reduction in the ultimate tensile strength and elongation of the IN713LC samples after the solid solution heat treatment. Nonetheless, the mechanical properties of the solid solution heat-treated IN713LC sample are still comparable to those of the as-cast sample.
- The EBSD and SEM analysis results have shown the existence of two cracking mechanisms in the as-built IN713LC components, namely solidification cracking due to compositional element segregation at the grain boundaries and ductility dip cracking (DDC) as a result of grain boundary sliding in successive layers of the built structure.

Overall, the present results have not only confirmed the feasibility of

processing IN713LC using LPBF but have also shown that the mechanical properties of the as-built components are better than those of the as-cast sample. Although the solid solution heat treatment process yields a significant improvement in the yield strength but get a reduction in the ultimate tensile strength and elongation compared to those of the as-built specimen, all of the mechanical properties are still comparable to the casting one.

In addition, previous studies [26,27] have shown that the grains in SLM can be modified by using HIP, which transforms the grains into equiaxed grains and closes the internal cracks. Thus, in future studies, a similar approach will be applied to suppress the grain size and close internal cracks in LPBF-printed components, and it is expected that all of the mechanical properties of the IN713LC specimen by using HIP will be enhanced.

CRediT authorship contribution statement

M. Mohsin Raza: Investigation, Writing – original draft, Writing – review & editing. **Yu-Lung Lo:** Conceptualization, Writing – original draft, Writing – review & editing, Supervision, Project administration, Funding acquisition.

Declaration of competing interest

The authors declare that they have no known competing financial interests or personal relationships that could have appeared to influence the work reported in this paper.

Acknowledgments

The authors gratefully acknowledge the financial support provided to this study by the Ministry of Science and Technology of Taiwan under Grant No. MOST 107-2218-E-006-051. The study was also supported in part by the funding provided to the Intelligent Manufacturing Research Center (iMRC) at National Cheng Kung University (NCKU) by the Ministry of Education, Taiwan, and Headquarters of University Advancement. The assistance provided by Prof. Fei-Yi Hung of NCKU in conducting the heat treatment and tensile testing elements of the present study is much appreciated.

References

[1] Z. Zhu, H. Basoalto, N. Warnken, R. Reed, A model for the creep deformation behaviour of nickel-based single crystal superalloys, Acta Mater. 60 (12) (2012) 4888–4900.
[2] M.J. Donachie, S.J. Donachie, Superalloys: a Technical Guide, ASM international, 2002.
[3] M. Henderson, D. Arrell, R. Larsson, M. Heobel, G. Marchant, Nickel based superalloy welding practices for industrial gas turbine applications, Sci. Technol. Weld. Join. 9 (1) (2004) 13–21.
[4] N.J. Harrison, Selective Laser Melting of Nickel Superalloys: Solidification, Microstructure and Material Response, University of Sheffield, 2016.
[5] S. Kou, Welding Metallurgy, New Jersey, USA, 2003, pp. 431–446.
[6] J. Risse and C. Broeckmann, "Additive manufacturing of nickel-base superalloy IN738LC by laser powder bed fusion," Lehrstuhl für Lasertechnik2019.
[7] S. Griffiths, et al., Combining alloy and process modification for micro-crack mitigation in an additively manufactured Ni-base superalloy, Additive Manufacturing 36 (2020), 101,443.
[8] N. Perevoshchikova, et al., Optimisation of selective laser melting parameters for the Ni-based superalloy IN-738 LC using Doehlert's design, Rapid Prototyping Journal, 2017.
[9] T. Maccagno, A. Koul, J.-P. Immarigeon, L. Cutler, R. Allem, G. L'esperance, Microstructure, creep properties, and rejuvenation of service-exposed alloy 713C turbine blades, Metallurgical Transactions A 21 (12) (1990) 3115–3125.
[10] B.B. Galizoni, A.A. Couto, D.A.P. Reis, Heat treatments effects on nickel-based superalloy inconel 713C, Metals 9 (1) (2019) 47.
[11] J.-R. Zhao, F.-Y. Hung, T.-S. Lui, Microstructure and tensile fracture behavior of three-stage heat treated inconel 718 alloy produced via laser powder bed fusion process, Journal of Materials Research and Technology 9 (3) (2020) 3357–3367.
[12] A. Standard, E8/E8M, Standard Test Methods for Tension Testing of Metallic Materials, vol. 3, 2011, p. 66.
[13] J.S. Cantó, S. Winwood, K. Rhodes, S. Birosca, A study of low cycle fatigue life and its correlation with microstructural parameters in IN713C nickel based superalloy, Mater. Sci. Eng., A 718 (2018) 19–32.
[14] M. Sadowski, L. Ladani, W. Brindley, J. Romano, Optimizing quality of additively manufactured Inconel 718 using powder bed laser melting process, Additive Manufacturing 11 (2016) 60–70.
[15] L.J. Ladani, A. Dasgupta, I. Cardoso, E. Monlevade, Effect of selected process parameters on durability and defects in surface-mount assemblies for portable electronics, IEEE Trans. Electron. Packag. Manuf. 31 (1) (2008) 51–60.
[16] N.J. Harrison, I. Todd, K. Mumtaz, Reduction of micro-cracking in nickel superalloys processed by Selective Laser Melting: a fundamental alloy design approach, Acta Mater. 94 (2015) 59–68.
[17] H. Wang, et al., Selective laser melting of the hard-to-weld IN738LC superalloy: efforts to mitigate defects and the resultant microstructural and mechanical properties, J. Alloys Compd. 807 (2019) 151662.
[18] Z. Wang, K. Guan, M. Gao, X. Li, X. Chen, X. Zeng, The microstructure and mechanical properties of deposited-IN718 by selective laser melting, J. Alloys Compd. 513 (2012) 518–523.
[19] X. Zhou, et al., Textures formed in a CoCrMo alloy by selective laser melting, J. Alloys Compd. 631 (2015) 153–164.
[20] S. Li, Q. Wei, Y. Shi, Z. Zhu, D. Zhang, Microstructure characteristics of Inconel 625 superalloy manufactured by selective laser melting, J. Mater. Sci. Technol. 31 (9) (2015) 946–952.
[21] L.N. Carter, M.M. Attallah, R.C. Reed, Laser powder bed fabrication of nickel-base superalloys: influence of parameters; characterisation, quantification and mitigation of cracking, Superalloys 2012 (2012) 577–586.
[22] P. Gao, et al., Cracking behavior and control of β-solidifying Ti-40Al-9V-0.5 Y alloy produced by selective laser melting, J. Mater. Sci. Technol. 39 (2020) 144–154.
[23] W. Zhou, et al., Inhibition of cracking by grain boundary modification in a non-weldable nickel-based superalloy processed by laser powder bed fusion, Materials Science and Engineering: A 791 (2020) 139,745.
[24] R. Rosenthal, D.R.F. West, Continuous γ′ precipitation in directionally solidified IN738 LC alloy, Mater. Sci. Technol. 15 (12) (1999) 1387–1394.
[25] A. Chamanfar, M. Jahazi, A. Bonakdar, E. Morin, A. Firoozrai, Cracking in fusion zone and heat affected zone of electron beam welded Inconel-713LC gas turbine blades, Mater. Sci. Eng., A 642 (2015) 230–240.
[26] C. Chen, et al., Effect of hot isostatic pressing (HIP) on microstructure and mechanical properties of Ti6Al4V alloy fabricated by cold spray additive manufacturing, Additive Manufacturing 27 (2019) 595–605.
[27] M.L. Montero-Sistiaga, S. Pourbabak, J. Van Humbeeck, D. Schryvers, K. Vanmeensel, Microstructure and mechanical properties of Hastelloy X produced by HP-SLM (high power selective laser melting), Materials & Design 165 (2019) 107,598.